Electrochimica Acta 394 (2021) 139055

Contents lists available at ScienceDirect

Electrochimica Acta

journal homepage: www.elsevier.com/locate/electacta

Exploring multivalent cations-based electrolytes for CO_2 electroreduction

Saket S. Bhargava[a,b,1], Emiliana R. Cofell[b,c,1], Prithviraj Chumble[a], Daniel Azmoodeh[a], Sujay Someshwar[a], Paul J.A. Kenis[a,b,*]

[a] Department of Chemical & Biomolecular Engineering, University of Illinois Urbana-Champaign (UIUC), United States
[b] International Institute for Carbon Neutral Energy Research (WPI-I2CNER), Kyushu University, Japan
[c] Department of Materials Science & Engineering, University of Illinois Urbana-Champaign (UIUC), United States

ARTICLE INFO

Article history:
Received 19 July 2021
Accepted 3 August 2021
Available online 10 August 2021

Keywords:
Carbon dioxide
Electrochemical reduction
Multivalent cations
Electrolyte composition
Surface deposits

ABSTRACT

Electrochemical reduction of CO_2 (CO_2RR) to value-added chemicals is a promising, potentially carbon-neutral alternative to the existing thermochemical fossil fuels-based, carbon-positive chemical manufacturing processes. The CO_2 electrolysis field has devoted significant attention to the effects of electrolyte composition and concentration on the rates and selectivities of the desired products; however, the effects of multivalent cations have not been widely studied. Here, we explore the feasibility of using multivalent cations-based electrolytes to intensify CO_2RR electrochemical performance. We provide experimental evidence that electrolytes containing multivalent cations, in contrast to those containing monovalent alkali metal cations, hinder the rates and selectivities for CO production on Ag nanoparticles. To explain these trends, we explore the possible origin of the reduced CO_2RR performance in the presence of multivalent cations-based electrolytes. Using a combination of electrochemical (electrochemical impedance spectroscopy) and physicochemical (grazing incidence X-ray diffraction, scanning electron microscopy, and energy dispersive X-ray spectroscopy) characterization methods, we provide evidence that in the presence of multivalent cations metal oxides and/or metal hydrides deposit on the electrode surface, possibly blocking the catalytically active sites, and thus impairing the adsorption of CO_2 on the catalyst surface.

1. Introduction

Electrochemical reduction of CO_2 (CO_2RR) to value-added carbon-based chemicals such as carbon monoxide, ethylene, and ethanol is emerging as a promising alternative to the conventional thermochemical fossil fuel-based industrial production methods [1–3]. Over the past decade, significant research progress has resulted in better fundamental understanding of the CO_2RR process [4–10]. Researchers have also explored reactor concepts for high rate, selective, and energy efficient CO_2RR to desired products [9,11–17]. In particular, the effects of composition and concentration of aqueous electrolytes on rates and selectivities for CO_2RR as well as on the degradation of electrodes have been studied in great detail computationally [18–20] and experimentally [16,21–24,52].

The role of alkali metal cations has been explained using various effects such as the promoter effect [16,19], the Frumkin effect [22], or using concepts based on cation hydrolysis [20], and CO desorption from the electrode surface [16]. The role of anions has been explained using concepts based on specific adsorption [21] and pH-based overpotential requirement [16,25]. However, no cation or anion effect is universal in nature, and each can only be used to explain certain trends, e.g., the Frumkin effect can only be used to explain the differences in electrochemical performance for different concentrations of the same cation but cannot be used to compare different cations even at the same concentration. In contrast, to the best of our knowledge, to date only four publications have reported insights on aqueous electrolytes containing multivalent cations [18,26–28]. Use of multivalent cations-based electrolytes (MVCEs) is particularly interesting for the CO_2RR field because such electrolytes are significantly cheaper than the more commonly used alkali metal cations-based electrolytes (AMCEs). Some prior studies report that CO_2RR is more active in the presence of multivalent cations as compared to alkali metal cations [18,26]. Combining the use of scalable gas diffusion electrode (GDE)-based flow electrolysis technology with MVCEs would result in lowered costs, and increased rates and selectivities for the desired products at industrial scales.

* Corresponding author.
E-mail address: kenis@illinois.edu (P.J.A. Kenis).
[1] These authors contributed equally to this work.

https://doi.org/10.1016/j.electacta.2021.139055
0013-4686/

Table 1
pH and conductivity values for the various electrolytes used in this study.

Salt	Concentration (mol/lit)	Density (kg/lit)	Concentration (mol/kg)	pH	Conductivity (mS/cm)	Refs.
NaCl	3	–	–	6.42	153.1	[16]
KCl	3	–	–	6.82	191.2	[16]
CsCl	3	–	–	7.24	207.8	[16]
$MgCl_2$	3	1.21	2.48	5.00	148.1	This work
$CaCl_2$	3	1.25	2.4	3.59	197.7	This work
$BaCl_2$	1.35	1.24	1.09	4.92	165.6	This work
$AlCl_3$	1.8	1.25	1.44	2.38	113.6	This work

Schizodimou and Kyriacou report the use of MVCEs on Cu-Sn-Pb alloy electrodes for CO_2RR [26]. At lower overpotentials, they observed that the rate of CO_2RR generally increased with the surface charge of the cation. They attributed the accelerating effect of the multivalent cations to the additional stabilization of the $CO_2^{\cdot-}$ radical in the rate determining step [26]. At higher overpotentials, the accelerating effect of the multivalent cations was not pronounced, an observation they attributed to a change in the rate determining step [26]. In this study, the MVCEs were used as supporting electrolytes in acidic media. Thus, the trends and effects observed in this study might not apply to cases where MVCEs in higher concentrations result in solutions with different pH values.

Ringe et al. report a multiscale model based on size-modified Poisson-Boltzmann theory and *ab initio* simulations of field effects on reaction intermediates generated during CO_2RR [18]. Their model predicts that CO_2RR in MVCEs can exhibit activity up to two orders of magnitude higher than in AMCEs. They rationalized the beneficial effect of using MVCEs as the net result of two competing effects: an increase in the interfacial field due to the larger charge and a decrease in the interfacial field due to larger size. However, they also point out that ion-correlation effects or chemical ion-adsorbate interactions might lead to deviations from the proposed simplified model, aspect that could be elucidated further with experiments.

Hussain et al. pursued the use of IR spectroscopy combined with capacitance measurements and *ab initio* molecular dynamics to demonstrate that in CO_2RR the location of the outer Helmholtz plane is determined by the size of the multivalent cations. They also posit that the cations influence the polarization and polarizability of the adsorbed CO species and the accumulation of electronic density of the O-atom of the adsorbed CO affecting its adsorption energy [27]. Their spectroscopic data also indicates that the degree of H-bonding of interfacial water to the adsorbed CO, and the degree of polarization of water molecules in the cation's solvation shell affect the CO_2RR mechanism. However, this study mostly utilized low electrolyte concentrations over intermediate potentials while noting that deviations are observed when running CO_2RR at more negative potentials. Thus, the results presented here might not explain the trends observed with very high electrolyte concentrations and/or under highly negative potentials.

Waegele et al., in a theoretical study, explained the impacts of multivalent cations on the CO_2RR mechanism by qualitatively analyzing the specific adsorption or quasi-specific adsorption behavior of the cations and the associated impacts on the bulk and interfacial water [28]. These interesting insights would need to be supplemented with experimental evidence for a general trend to be confirmed.

In this work, we study the electrochemical reduction of CO_2 on Ag nanoparticles (NPs)-based GDEs in a flow electrolysis configuration in the presence of chloride-based electrolytes with alkali metal and multivalent cations. The intent of this study is to explore the feasibility of using MVCEs in the CO_2 electrolysis process and not to unravel the fundamental electrokinetic role(s) of the multivalent cations on CO_2RR. Experiments presented herein indicate that the electrochemical performance for CO_2RR to CO is significantly worse in the presence of electrolytes containing multivalent cations as compared to electrolytes containing monovalent alkali metal cations. We report extensive electrochemical (electrochemical impedance spectroscopy – EIS) and physicochemical (grazing incidence X-ray diffraction – GIXRD, scanning electron microscopy – SEM, energy dispersive X-ray spectroscopy – EDX) characterizations to elucidate the effects of multivalent cations on CO_2RR leading to poor electrochemical performance for CO production.

2. Experimental

2.1. Preparation of electrolytes

The preparation of NaCl, KCl, and CsCl electrolyte solutions is outlined in our prior work [16]. For this work, we prepared electrolyte solutions of commercially available $MgCl_2$, $CaCl_2$, $BaCl_2$, and $AlCl_3$ salts. The desired electrolyte concentrations were achieved by dissolving the appropriate amounts of salts in Barnstead E-pure water ($>$ 18 MΩ cm). The following salts were used: $MgCl_2$ (product number: M9272, assay: 99.0 – 102.0%, Sigma Aldrich), $CaCl_2$ (product number: 442909, assay: 98%, Sigma Aldrich), $BaCl_2$ (product number: 217565, assay: $\geq$ 99%, Sigma Aldrich), and $AlCl_3$ (product number: 237078, assay: 99%, Sigma Aldrich). The salts were used without any further purification.

2.2. pH and conductivity measurements

The pH and conductivity values for the AMCE solutions were taken from our prior work [16]. For the MVCE solutions, the pH and conductivity values were measured using an Orion 4-star pH-conductivity meter at room temperature. For pH calibration, we used buffer solution standards of pH 4, 7, and 10 (product numbers: SB101, SB107, and SB115, Fisher Chemical) and for conductivity calibration, we used Orion conductivity standards of 1413 μS/cm and 111.9 mS/cm (product numbers: 011007 and 011005, ThermoFisher Scientific). The pH and conductivity values of the electrolyte solutions are listed in Table 1 below. The density for $AlCl_3$ solution was taken from the link [29] and the densities for $MgCl_2$, $CaCl_2$, and $BaCl_2$ solutions were taken from a property estimation website [30]. The target concentration for all electrolytes was 3 M so that comparison with prior work could be easily made [16]. However, $BaCl_2$ and $AlCl_3$ ran into solubility limitations, and thus had to be tested at lower concentrations. Since our focus in this study is on performance trends, the results of this study can be compared qualitatively.

2.3. Preparation of GDEs

The Ag and IrO_2 gas diffusion electrodes (GDEs) were prepared by spraying the catalyst ink on Sigracet 39 BCE gas diffusion layers (GDLs) (product code: 1592011, Fuel Cell Store) using an automated

airbrushing setup as previously reported [31]. Four electrodes were prepared at a time. Commercially available Ag nanoparticles (product number: 576832, size: < 100 nm, purity: 99.5% trace metals basis, Sigma Aldrich) were used as the cathode catalyst and commercially available IrO_2 nanoparticles (product number: 43396–06, purity: 99.99% metals basis, Ir 84.5% min., Alfa-Aesar). The targeted catalyst loadings for Ag nanoparticles and IrO_2 nanoparticles were 2 mg/cm^2 and 3 mg/cm^2, respectively. The catalyst inks were prepared by mixing appropriate amounts of nanoparticles with 2400 μL of Barnstead E-pure water (> 18 MΩ cm), certain amounts of Nafion solution (product number: NS05, 5 wt%, Fuel Cell Earth), and 2400 μL of isopropyl alcohol (IPA). The mixture was then sonicated (Vibra-Cell ultrasonic processor, Sonics & Materials) for at least 20 min and then airbrushed onto a GDL with a geometric area of 5 × 2 cm^2. The amounts of catalysts and Nafion solution used were 40 mg, 104 μL and 60 mg, 195 μL for Ag and IrO_2 catalysts, respectively. The actual catalyst loadings were determined by weighing the GDLs before and after the deposition. The final catalyst loadings were 2 ± 0.2 mg/cm^2 and 3 ± 0.3 mg/cm^2, respectively, for Ag and IrO_2 catalyst GDEs.

2.4. Electrochemical flow reactor operation

All electrochemical experiments were performed in a flow reactor reported earlier, under ambient conditions [16]. A fresh GDE was used for all experiments. The gas flow fields, liquid flow fields, and the GDEs were all 1 cm^2 in geometric area. A mass flow controller (Smart Trak 2, Sierra Instruments) was used to control the flow rate of CO_2 gas (Airgas UN 1013) at 17 sccm. A syringe pump (Pump 33, Harvard Apparatus) was used to control the electrolyte flow rate at 1 mL/min. The gaseous products were analyzed by an inline GC and the transfer of gaseous products from the cathode to the GC was facilitated using a pressure controller (Cole Parmer, 00268TC) to control the reactor downstream pressure at 14.20 psia. A potentiostat (Metrohm Autolab PGSTAT302N) was used to apply potentials. Cell potential was controlled for all potentiostatic experiments. To measure the potentials of the individual electrodes, a multimeter (Hyelec MS8233D) was connected between the electrode and the reference electrode (Ag/AgCl; 3 mol/kg, RE-5B, BASi) as shown in our previous work [32]. The reference electrode was placed in the inlet stream of the electrolyzer to avoid the effect of any pH changes that may occur in the flow cell as a function of the applied potential. The potentials are reported in this study without any iR-correction. After applying a potential, the current was allowed to stabilize for at least 120 s before the gas product analysis was performed. The protocol for gaseous stream analysis is detailed in the section below. No liquid products were analyzed for this study. Current densities fluctuated due to the formation of gas bubbles and thus, the current densities were averaged over a time period of at least 180 s. The CO Faradaic Efficiency (FE) was calculated using the following relation: CO FE (%) = (2*n*F/Q)*100 where n is the number of moles of product formed, F is the Faraday's constant (96,485 C mol^{-1}), and Q is the total amount of charge passed. The CO partial current density (j_{CO}) was then obtained by multiplying the total current density (j_{total}) with the CO FE.

2.5. Electrochemical impedance spectroscopy measurements

EIS was performed on the flow cell using the EIS module of a different potentiostat (Reference 600, Gamry). The spectra were recorded in galvanostatic mode at −1 mA and −10 mA. 14 points per decade were scanned in the range from 10 kHz to 0.1 Hz after an initial delay of 20 s. A single sine wave with an amplitude of 1 mA RMS was used for the sweep.

2.6. Analysis of gaseous products using an inline GC

The gaseous product stream was analyzed by a method previously reported by us [16]. Briefly, 0.5 mL of the effluent gas stream was sampled into a Thermo Finnigan Trace GC. Three injections were made 90 s apart during the same run to average out the gaseous product peaks over time. A 60/80 Carboxen 1000 SS packed column (12390-U Supelco, Sigma Aldrich) was used. The thermal conductivity detector (TCD) was used with Helium (Airgas UN 1046) as the carrier gas at a flow rate of 30 sccm. The oven was held at 150 °C and the TCD at 200 °C. Appropriate calibration curves were used to determine the actual concentrations.

2.7. Physicochemical characterizations

Electrodes were characterized pre-testing and post-testing – both with and without a post-testing rinse (ten seconds with DI water, dried with N_2).

2.7.1. X-ray diffraction (XRD) measurements

Bulk powder X-ray diffraction (PXRD) and grazing incidence X-ray diffraction (GIXRD) characterizations were performed for the GDEs post-testing (with and without a post-testing rinse) using a Bruker D8 Advance XRD System, which was operated at 40 kV and 40 mA. The GIXRD measurements were performed at an angle of theta= 1°, corresponding to a penetration depth of approximately 14 μm, which is within the thickness of catalyst layer (30–40 μm) (see SI for calculation information). XRD peaks were analyzed using Jade software and peaks were matched with the powder diffraction database from the International Center for Diffraction Data's PDF 4 + 2021 software.

2.7.2. Scanning electron microscope (SEM) and energy-dispersive X-ray spectroscopy (EDX) measurements

Fresh GDEs and GDEs post-testing (with and without a post-testing rinse) were imaged using a scanning electron microscope (SEM) (FEI Quanta FEG 450 ESEM); the microscope was operated at 15 kV and images were taken at 80x, 250x, 500x, 1000x, and 5000x magnifications in order to compare the overall surface morphology as well as the microscale structure after testing in the various electrolytes. Energy-dispersive X-ray spectroscopy (EDX) (FEI Quanta FEG 450 ESEM) was performed using the same instrument; both point and mapping analyses were performed on the surface to detect the presence of elements.

3. Results & discussion

The focus of this study is to investigate the effect of MVCEs on CO_2RR, and to compare our observations with our previously collected data on AMCEs in a prior study [16]. The electrolyte concentration was 3 M for all electrolytes except for $BaCl_2$ and $AlCl_3$ solutions due to solubility limitations. However, because the focus in this work is on performance comparison rather than quantitative comparison, the results of this study can be compared qualitatively. We use multivalent metal chlorides in this study because other salts for all the cations used in this study are either not naturally stable or insoluble in water. In all experiments, high catalyst loadings, high electrolyte stream and CO_2 stream flow rates, and high electrolyte concentrations are used to minimize mass transport and conductivity limitations. The intent of this study is to assess the feasibility of using MVCEs in the CO_2 electrolysis process and not to unravel the fundamental kinetics of CO_2RR in the presence of MVCEs.

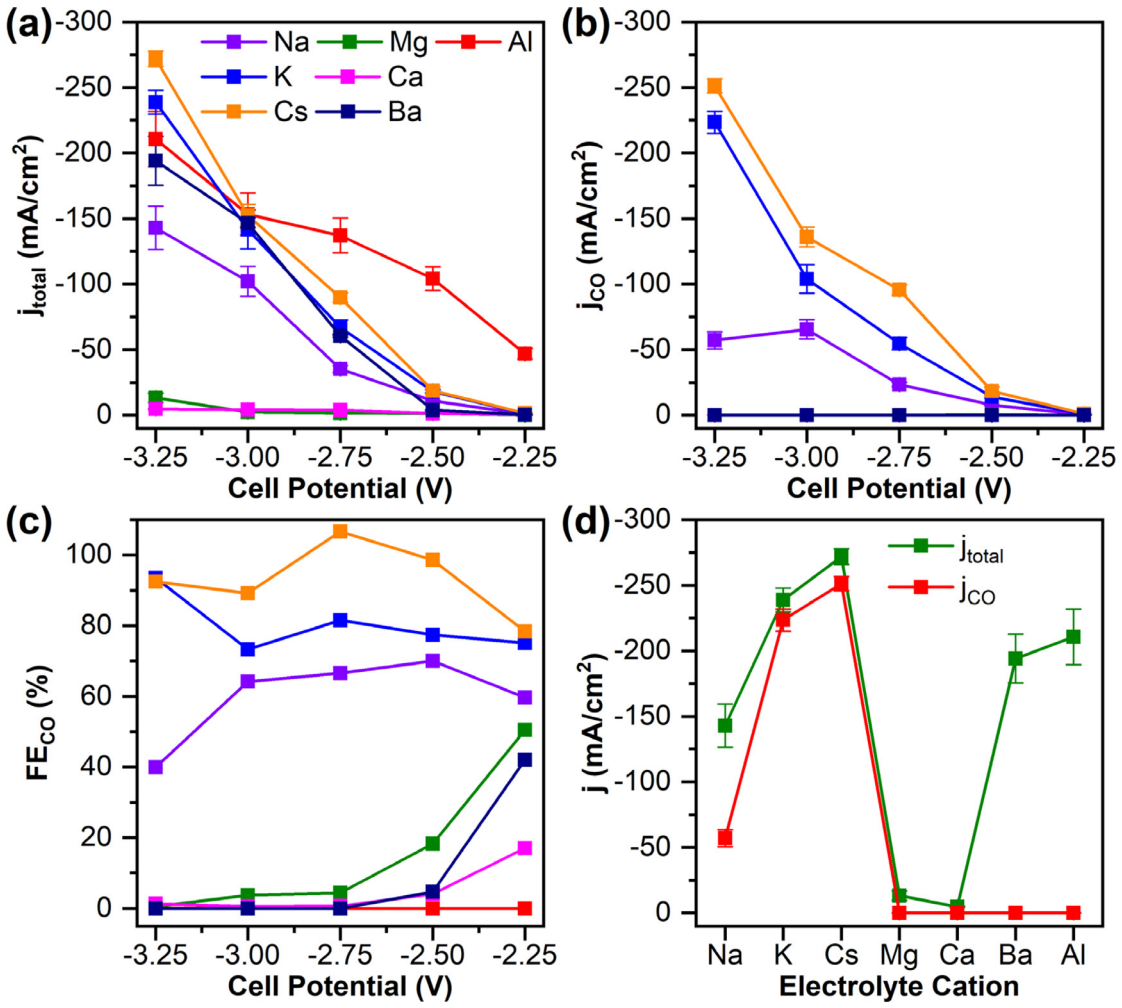

Fig. 1. j-V curves obtained in MCl_x (M = Na, K, Cs (x = 1) or Mg, Ca, Ba (x = 2) or Al (x = 3)) electrolytes: **(a)** j_{total} obtained as a function of the cell potential; **(b)** j_{CO} obtained as a function of the cell potential; **(c)** CO FEs obtained as a function of the cell potential; **(d)** j_{total} and j_{CO} obtained as a function of the different electrolyte cations used in this study. These curves show that alkali metal cations-based electrolytes have a promotional effect on CO_2RR performance whereas multivalent cations-based electrolytes hinder the CO_2RR performance. In all cases, an Ag GDE was used as the cathode and an IrO_2 GDE was used as the anode with catalyst loadings of 2 mg/cm^2 and 3 mg/cm^2, respectively. The flow rates of electrolyte and CO_2 were 1 mL/min and 17 sccm, respectively. The concentrations of the different electrolyte solutions are listed in Table 1.

3.1. Effects of multivalent cation-based electrolytes on CO_2RR to CO on Ag NPs

Fig. 1 shows the electrochemical performance of CO_2RR to CO in the presence of different electrolytes. Fig. 1a shows the j_{total} measured as a function of the cell potential for different electrolytes. The trends show that for AMCEs, the j_{total} increases as: $Cs^+ > K^+ > Na^+$, whereas for MVCEs, the j_{total} follows the following trend: $Al^{3+} > Ba^{2+} > Mg^{2+} \approx Ca^{2+}$. Combining these observations, the overall trend for j_{total} is as follows: $Cs^+ > K^+ > Al^{3+} > Ba^{2+} > Na^+ > Mg^{2+} \approx Ca^{2+}$. Fig. 1b shows the j_{CO} measured as a function of the cell potential for all different electrolytes. The j_{CO} for AMCEs increases in the same order: $Cs^+ > K^+ > Na^+$, however, for MVCEs, the j_{CO} follows a different trend: $Al^{3+} \approx Ba^{2+} \approx Mg^{2+} \approx Ca^{2+} \approx 0$. Combining these observations, the overall trend for j_{CO}: $Cs^+ > K^+ > Na^+ > Al^{3+} \approx Ba^{2+} \approx Mg^{2+} \approx Ca^{2+}$. Fig. 1c shows the CO FEs obtained as a function of the cell potential for the different electrolytes. The trends show that for AMCEs, the CO FE increases as follows: $Cs^+ > K^+ > Na^+$ for low and high cell potentials, whereas for MVCEs, the CO FE follows a different trend: $Mg^{2+} > Ba^{2+} > Ca^{2+} > Al^{3+}$ at low cell potentials and $Mg^{2+} > Ba^{2+} \approx Ca^{2+} \approx Al^{3+} \approx 0$ at high cell potentials. Combining these observations, the overall trend for CO FE is: $Cs^+ > K^+ > Na^+ > Mg^{2+} > Ba^{2+} > Ca^{2+} > Al^{3+}$ at low cell potentials and $Cs^+ > K^+ > Na^+ > Mg^{2+} > Ba^{2+} \approx Ca^{2+} \approx Al^{3+}$ at high cell potentials. We also compared the j_{total} and j_{CO} obtained as a function of the electrolyte cation at a cell potential of −3.25 V (Fig. 1d). This comparison highlights that the measured j_{CO} values are strongly influenced by the electrolyte cation and are higher for electrolytes containing alkali metal cations, while the j_{CO} values are less than 1 mA/cm^2 for electrolytes containing multivalent cations. This suggests that the CO_2RR is being hindered in the presence of multivalent cations, which could be due to either (i) mechanistic impacts such as impaired CO_2 adsorption, destabilization of the $CO_2^{\cdot-}$ intermediate, and/or hindered CO desorption, or (ii) electrode/catalyst surface passivation as a result of the formation of thin films that block the active catalyst sites, or (iii) both (i) and (ii). In the next sections we investigate these possible causes for the observed hampered CO_2RR performance in the presence of MVCEs. The electrochemical performance of the hydrogen evolution reaction (HER) is shown in Fig. S1 in the supplementary information (SI). The j-V curves as a function of the cathode potential (measured vs. Ag/AgCl) are shown in Fig. S2 in the SI. We would also like to point out that the sum of CO FEs and hydrogen FEs does not equal to (or reach close to) 100%.

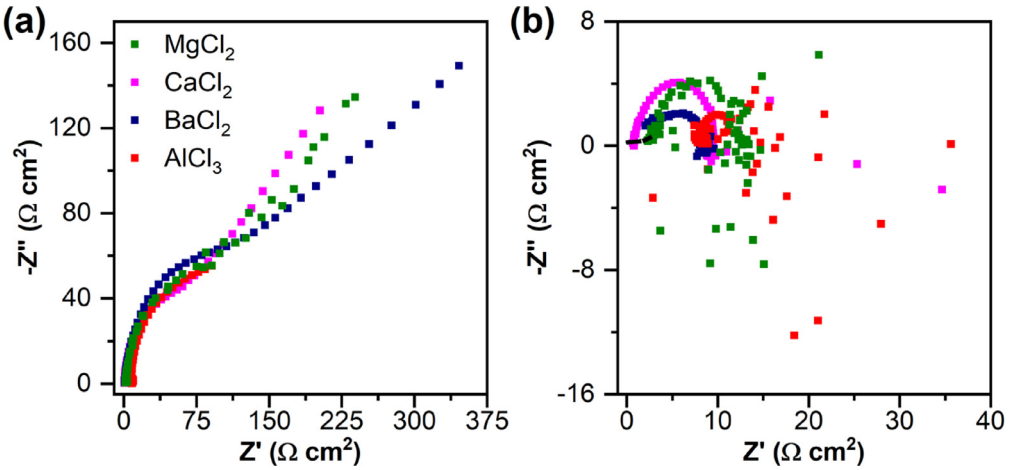

Fig. 2. Galvanostatic electrochemical impedance spectroscopy of a GDE-based flow cell system operated with MCl_x electrolytes (M = Mg, Ca, Ba (x = 2) or Al (x = 3)) electrolytes: **(a)** Nyquist plots obtained at an applied current of −1 mA; **(b)** Nyquist plots obtained at an applied current of −10 mA. These curves show that at low currents, the CO_2RR process is diffusion-limited whereas at high currents, the CO_2RR process is limited by surface passivation. In all cases, an Ag GDE was used as the cathode and an IrO_2 GDE was used as the anode with catalyst loadings of 2 mg/cm^2 and 3 mg/cm^2, respectively. The flow rates of the electrolyte and CO_2 streams were 1 mL/min and 17 sccm, respectively. Table 1 lists the concentrations of the different electrolyte solutions.

We hypothesize that this is due to the formation of various surface deposits as side Faradaic reactions (explored further in sections below). Figs. S3, S4, and S5 in the SI examine the dependence of j_{total}, j_{CO}, and CO FE, respectively on the various electrolyte properties (such as pH, conductivity, hydrated cation radius, and cation crystal radius). The key takeaway from these graphs is that j_{total} does not follow any specific trends with respect to any of the electrolyte properties listed above whereas the j_{CO} and the CO FE are a strong function of the electrolyte pH and the hydrated cation radius but do not follow any specific trends with respect to the electrolyte conductivity or the crystal radius of the electrolyte cation. In general, the j_{CO} and the CO FE increase with increase in the electrolyte pH and decrease in the hydrated cation radius.

3.2. Elucidating the role of multivalent cations in CO_2RR to CO on AG NPs

3.2.1. Electrochemical characterizations in MCl_x electrolytes

Despite the gaps in the understanding of the mechanism of CO_2RR, the importance of CO_2 adsorption on the electrode surface is clear because all subsequent steps in the mechanism will be affected by this CO_2 adsorption step. Similarly, the CO desorption step is also important because the rate of desorption of CO from the electrode surface directly affects the electrochemical performance. Fig. 2 shows the galvanostatic electrochemical impedance spectroscopy (GEIS) measurements for the GDE-based flow cell setup operated with the different electrolytes. The Nyquist plots presented in Fig. 2a imply that the CO_2RR process is limited by CO_2 diffusion to the catalyst surface in the presence of MVCEs [33–35]. These diffusion limitations will impact subsequent steps in the reaction and can explain the low activity (j_{CO}) and selectivity (CO FE) at low currents. In contrast, in our prior work EIS studies for CO_2RR in AMCEs do not show diffusion-limited behavior; instead, they show evidence of kinetic limitations [16,21]. This also suggests that the higher j_{total} values observed despite CO_2 diffusion limitations are a result of unwanted Faradaic reactions (such as the formation of some surface species as explored further in the next section).

The Nyquist plots presented in Fig. 2b collected (collected at a higher current of −10 mA) imply that the CO_2RR process is limited either by impaired CO_2 adsorption or surface passivation, or a combination of both, in the presence of MVCEs [33–35]. Passivation of the electrode surface could cause the active catalyst sites to be blocked, thus hindering the adsorption of CO_2, which in turn retards the rates of subsequent steps. This electrode surface passivation can explain the low selectivity at high currents. In contrast, prior studies suggest the presence of an electron transfer step or the CO desorption step to be rate determining for CO_2RR in AMCEs [7,9,10,16,36,37].

To further investigate the presence and nature of surface deposits formed at high current densities we studied the Pourbaix diagrams – simulated using materialsproject.org – for the various MVCEs used in our study [38–40]. When we simulated Pourbaix diagrams, we observed that the electrolyte concentration had a significant effect on the possible species that could exist. Thus, it would not be possible to predict with certainty the results of this study without performing both electrochemical experiments and physicochemical characterizations. Table 1 lists the pH and conductivity for all electrolytes used in this study. Pourbaix diagrams indicate the presence of solid metal oxides and metal hydrides on the electrode surface under the highly reducing operation conditions during CO_2RR (Fig. 3a–d). If indeed present, these surface deposits can block the active catalyst sites and thus hinder CO_2 adsorption. Further physicochemical characterization was performed to provide evidence for these claims: we analyze the GDEs using GIXRD, SEM, and EDX characterization techniques as discussed in the next section.

3.2.2. Physicochemical surface characterizations of GDEs

We performed both bulk and grazing incidence (GI) XRD on electrodes after electrochemical testing with the different AMCEs and MVCEs. Analysis was performed on samples that underwent one of two post-treatments: (1) samples were removed from the cell and left to dry to preserve post-testing electrolyte compounds and conditions (“unrinsed”), or (2) samples were thoroughly rinsed with DI water for ten seconds and then dried under nitrogen (“rinsed”). Rinsing the GDEs post-testing allowed us to isolate which compounds were adsorbed on the electrode surface during testing rather than adsorbed upon crystallization as the electrolyte dried. All characterized electrodes were compared to a pristine, untested silver-painted GDE in order to determine changes in catalyst layer morphology and composition.

Both bulk and GIXRD show the presence of a variety of oxides, hydrides, and hydroxides on the rinsed electrodes post-testing in the different MVCEs. In comparison, electrodes operated in high-performing AMCEs (KCl and CsCl) do not exhibit oxides, hydrides,

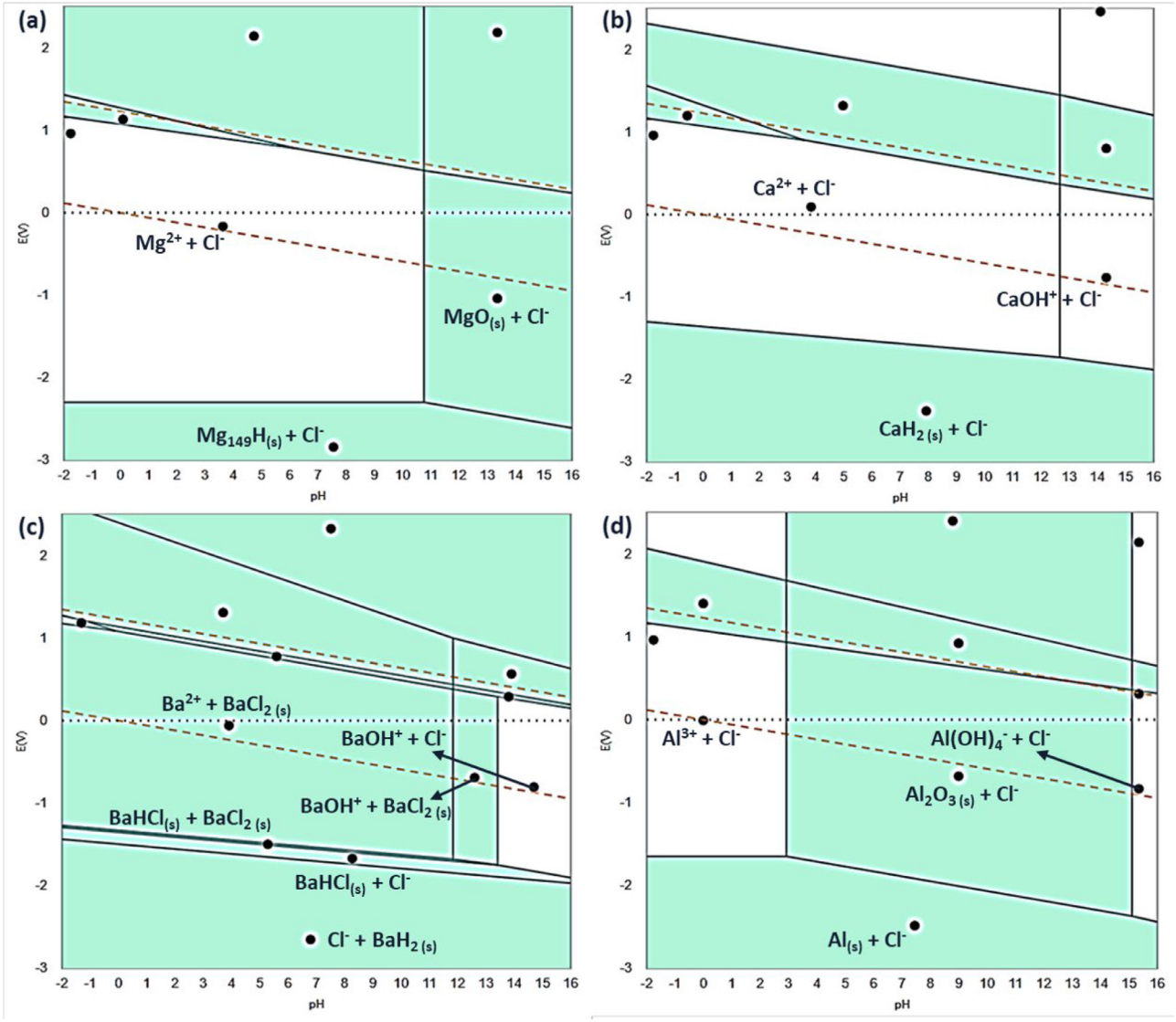

Fig. 3. Pourbaix diagrams for MCl_x electrolytes (M = Mg, Ca, Ba (x = 2) or Al (x = 3)) electrolytes: **(a)** 3 M $MgCl_2$; **(b)** 3 M $CaCl_2$; **(c)** 1.35 M $BaCl_2$; **(d)** 1.8 M $AlCl_3$. The Pourbaix diagrams are simulated from materialsproject.org. These Pourbaix diagrams suggest the possibility that surface deposits might be present on the catalyst surface under the operating conditions of CO_2RR.

and hydroxides on the surface. These bulk and GIXRD results for rinsed GDEs are presented in Fig. 4. Interestingly, the electrode operated in NaCl shows the presence of $Na_3H(CO_3)_2 \bullet H_2O$, a mineral known as trona, on the surface after testing, which may explain the lower performance of this electrolyte compared to KCl and CsCl.

Unrinsed GDEs exhibit multiple electrolyte peaks in addition to oxides, hydrides, and hydroxides; in some cases, these samples confirm the presence of these compounds but generally they are obscured due to high signal from the crystallized electrolyte. The bulk and GIXRD results for unrinsed GDEs are shown in Fig. S6 in the SI.

We also performed SEM to confirm the presence of various adsorbed deposits on the electrode surface after electrochemical testing; SEM images of all electrodes post testing can be found in Figs. S7 and S8. We additionally performed EDX on the samples to confirm the composition of surface deposits; EDX results for rinsed GDEs are shown in Figs. S9 and S10.

For GDEs tested in $AlCl_3$ we see peaks corresponding to the presence of Al_2O_3 (corundum); these peaks are more evident in unrinsed GDEs (Fig. S6). SEM analysis of both rinsed and unrinsed GDEs shows a deposit layer covering the surface of the catalyst layer, which exhibits similar morphology to Al_2O_3 reported in the literature (Figs. S7 and S8) [41,42]. The presence of oxygen in these surface deposits was confirmed via EDX (Figs. S9 and S10), lending additional evidence to oxide formation on the surface post testing.

XRD analysis of GDEs tested in $BaCl_2$ indicates the presence of a variety of compounds: barium hydroxide hydrate ($Ba(OH)_2 \bullet H_2O$), barium hydride (BaH_2), barium oxide (BaO and BaO_2), and barium carbonate ($BaCO_3$). While it is difficult to determine which compounds are most prevalent due to overlap in peak positions for many of these compounds, it is clear from this analysis that several of these compounds have been adsorbed and remain on the GDE surface post-testing. SEM images show the widespread presence of large-scale deposit layers and small (~1 μm) threadlike crystals in the catalyst layer that may be either $Ba(OH)_2$ or BaO (Figs. S7 and S8) [43–45]. This data suggests that the adsorption of these compounds explains the observed lack of electrochemical performance in $BaCl_2$ electrolyte (Fig. 1) due to active catalyst sites being blocked by adsorbed hydrides, oxides, and carbonates.

GDEs tested in $CaCl_2$ exhibit XRD peaks corresponding to calcium hydroxide ($Ca(OH)_2$), calcium oxide (CaO), calcium hydride

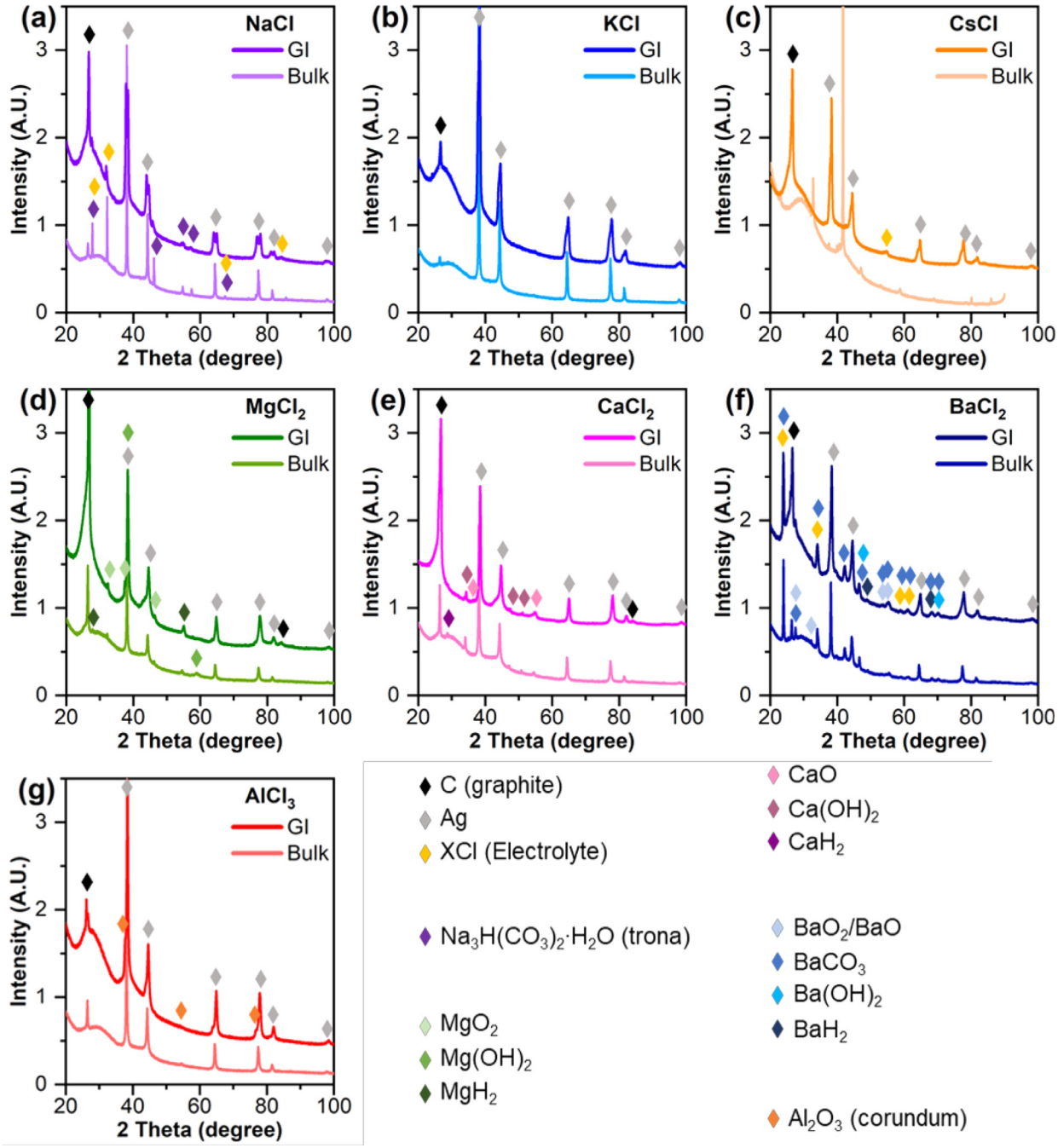

Fig. 4. Bulk and GIXRD measurements on GDE surfaces – rinsed post-testing in various electrolytes: **(a)** NaCl; **(b)** KCl; **(c)** CsCl; **(d)** $MgCl_2$; **(e)** $CaCl_2$; **(f)** $BaCl_2$; and **(g)** $AlCl_3$. XRD measurements confirm the presence of various surface deposits on the catalyst surface.

(CaH_2), and calcium carbonate ($CaCO_3$). SEM images of the washed GDE surface show widespread deposits once again, with ~1 μm crystals present on the surface (Figs. S7 and S8). These deposits are similar in morphology to both CaO and $Ca(OH)_2$ characterized in the literature and are broadly present across the GDE, obscuring the silver catalyst layer [46,47].

GDEs tested in $MgCl_2$ similarly exhibit peaks corresponding to magnesium hydroxide ($Mg(OH)_2$), magnesium oxide (MgO), magnesium hydride (MgH_2), and magnesium carbonate ($MgCO_3$). SEM images of washed GDEs show widespread surface deposits post-testing, leaving almost no visible areas of remaining catalyst layer. In these electrolytes, poor electrochemical performance (Fig. 1) can be explained by blockage of catalyst sites by these surface deposits.

GDEs tested in AMCEs (KCl and CsCl) do not exhibit XRD peaks corresponding to potassium and cesium oxides, hydrides, and hydroxides. SEM images indicate that most of the catalyst layer appears unobscured by deposits post testing. Some small deposits are visible at high magnification, which are similar in morphology to the carbonates observed in our previous work in K^+- and Cs^+-based electrolytes, but overall the catalyst layer appears pristine [52]. This, along with the observed excellent electrochemical performance in AMCEs (Fig. 1), further supports the explanation that adsorbed deposits block catalytic sites, leading to poor perfor-

mance in MVCEs. Moreover, the formation of oxide, hydride, and hydroxide deposits on the surface of electrodes in MVCEs is immediate and widespread, while carbonate deposit formation proceeds more gradually.

4. Conclusions & future work

In summary, we demonstrate that AMCEs and MVCEs have different effects on the CO_2RR performance on Ag NPs when used in an alkaline electrolyte-based flow cell. While alkali metal cations strongly promote the j_{CO} and CO FEs, multivalent cations hinder CO_2 adsorption on the electrode surface. The cation effects on CO production performance do not correlate with the electrolyte conductivity or the cation crystal radius but show a strong dependence on the electrolyte pH and the hydrated cation radius. Different cation groups behave differently and some of the previously proposed explanations for cation effects do not hold universally. To achieve CO_2RR performance of interest for applications, AMCEs should be used. Future experimental work should explore ways to prevent the formation of surface deposits in the presence of MVCEs. Strategies to avoid these surface deposits could be based on engineering the electrode-electrolyte interface [12,48,49], use of additives [50,51], and/or reactor and electrolyte engineering [52]. Preventing surface deposits in the presence of multivalent cations would help to fill gaps in understanding of multivalent cation effects on CO_2RR. Furthermore, this could confirm observed and proposed trends of multivalent cations on the CO_2RR from prior spectroscopic [27], theoretical [28], and/or modeling [18] work as summarized in the introduction. Building on prior work [18,28],[53–58], detailed investigations into the electrical double layer are also necessary.

Declaration of Competing Interest

The authors declare that they have no known competing financial interests or personal relationships that could have appeared to influence the work reported in this paper.

Acknowledgment

S.S.B would like to thank the Link Foundation for the providing the Link Energy Fellowship. We would like to thank the Beckmann Institute for Advanced Science and Technology Imaging Technology Group and the Frederick M. Seitz Materials Research Laboratory at UIUC; all physicochemical characterizations were carried out in these facilities.

Supplementary materials

Supplementary material associated with this article can be found, in the online version, at doi:10.1016/j.electacta.2021.139055.

References

[1] O.S. Bushuyev, P. De Luna, C.T. Dinh, L. Tao, G. Saur, J. van de Lagemaat, S.O. Kelley, E.H. Sargent, What should we make with CO_2 and how can we make it? Joule 2 (2018) 825–832.
[2] H.R.M. Jhong, S. Ma, P.J.A. Kenis, Electrochemical conversion of CO_2 to useful chemicals: current status, remaining challenges, and future opportunities, Curr. Opin. Chem. Eng. 2 (2013) 191–199.
[3] D.T. Whipple, P.J.A. Kenis, Prospects of CO_2 utilization via direct heterogeneous electrochemical reduction, J. Phys. Chem. Lett. 1 (2010) 3451–3458.
[4] E.L. Clark, S. Ringe, M. Tang, A. Walton, C. Hahn, T.F. Jaramillo, K. Chan, A.T. Bell, Influence of atomic surface structure on the activity of ag for the electrochemical reduction of CO_2 to CO, ACS Catal. 9 (2019) 4006–4014.
[5] M.R. Singh, J.D. Goodpaster, A.Z. Weber, M. Head-Gordon, A.T. Bell, Mechanistic insights into electrochemical reduction of CO_2 over Ag using density functional theory and transport models, Proc. Natl. Acad. Sci. U.S.A. 114 (2017) E8812–E8821.
[6] X. Wang, J.F. de Araújo, W. Ju, A. Bagger, H. Schmies, S. Kühl, J. Rossmeisl, P. Strasser, Mechanistic reaction pathways of enhanced ethylene yields during electroreduction of CO_2–CO co-feeds on Cu and Cu-tandem electrocatalysts, Nat. Nanotechnol. 14 (2019) 1063–1070.
[7] N.J. Firet, W.A. Smith, Probing the reaction mechanism of CO2 electroreduction over Ag films via operando infrared spectroscopy, ACS Catal. 7 (2017) 606–612.
[8] C.X. Zhao, Y.F. Bu, W. Gao, Q. Jiang, CO_2 Reduction mechanism on the Pb(111) surface: effect of solvent and cations, J. Phys. Chem. C 121 (2017) 19767–19773.
[9] Q. Lu, F. Jiao, Electrochemical CO_2 reduction: electrocatalyst, reaction mechanism, and process engineering, Nano Energy 29 (2016) 439–456.
[10] J. Rosen, G.S. Hutchings, Q. Lu, S. Rivera, Y. Zhou, D.G. Vlachos, F. Jiao, Mechanistic insights into the electrochemical reduction of CO_2 to CO on nanostructured Ag surfaces, ACS Catal. 5 (2015) 4293–4299.
[11] L.C. Weng, A.T. Bell, A.Z. Weber, Towards membrane-electrode assembly systems for CO_2 reduction: a modeling study, Energy Environ. Sci. 12 (2019) 1950–1968.
[12] F.P. García de Arquer, C.T. Dinh, A. Ozden, J. Wicks, C. McCallum, A.R. Kirmani, D.H. Nam, C. Gabardo, A. Seifitokaldani, X. Wang, Y.C. Li, F. Li, J. Edwards, L.J. Richter, S.J. Thorpe, D. Sinton, E.H. Sargent, CO_2 Electrolysis to multicarbon products at activities greater than 1 A cm^{-2}, Science 367 (2020) 661–666.
[13] C.M. Gabardo, C.P. O'Brien, J.P. Edwards, C. McCallum, Y. Xu, C.T. Dinh, J. Li, E.H. Sargent, D. Sinton, Continuous carbon dioxide electroreduction to concentrated multi-carbon products using a membrane electrode assembly, Joule 3 (2019) 2777–2791.
[14] C.M. Gabardo, A. Seifitokaldani, J.P. Edwards, C.T. Dinh, T. Burdyny, M.G. Kibria, C.P. O'Brien, E.H. Sargent, D. Sinton, Combined high alkalinity and pressurization enable efficient CO_2 electroreduction to CO, Energy Environ. Sci. 11 (2018) 2531–2539.
[15] C.T. Dinh, T. Burdyny, M.G. Kibria, A. Seifitokaldani, C.M. Gabardo, F.P. García de Arquer, A. Kiani, J.P. Edwards, P. De Luna, O.S. Bushuyev, C. Zou, R. Quintero-Bermudez, Y. Pang, D. Sinton, E.H. Sargent, CO₂ electroreduction to ethylene via hydroxide-mediated copper catalysis at an abrupt interface, Science, 360 (2018) 783.
[16] S.S. Bhargava, F. Proietto, D. Azmoodeh, E.R. Cofell, D.A. Henckel, S. Verma, C.J. Brooks, A.A. Gewirth, P.J.A. Kenis, System design rules for intensifying the electrochemical reduction of CO_2 to CO on Ag Nanoparticles, ChemElectroChem 7 (2020) 2001–2011.
[17] S.S. Bhargava, D. Azmoodeh, X. Chen, E.R. Cofell, A.M. Esposito, S. Verma, A.A. Gewirth, P.J.A. Kenis, Decreasing the energy consumption of the CO_2 electrolysis process using a magnetic field, ACS Energy Lett. (2021) 2427–2433.
[18] S. Ringe, E.L. Clark, J. Resasco, A. Walton, B. Seger, A.T. Bell, K. Chan, Understanding cation effects in electrochemical CO_2 reduction, Energy Environ. Sci. 12 (2019) 3001–3014.
[19] J. Resasco, L.D. Chen, E. Clark, C. Tsai, C. Hahn, T.F. Jaramillo, K. Chan, A.T. Bell, Promoter effects of alkali metal cations on the electrochemical reduction of carbon dioxide, J. Am. Chem. Soc. 139 (2017) 11277–11287.
[20] M.R. Singh, Y. Kwon, Y. Lum, J.W. Ager, A.T. Bell, Hydrolysis of electrolyte cations enhances the electrochemical reduction of CO_2 over Ag and Cu, J. Am. Chem. Soc. 138 (2016) 13006–13012.
[21] S. Verma, X. Lu, S. Ma, R.I. Masel, P.J.A. Kenis, The effect of electrolyte composition on the electroreduction of CO_2 to CO on Ag based gas diffusion electrodes, Phys. Chem. Chem. Phys. 18 (2016) 7075–7084.
[22] M.R. Thorson, K.I. Siil, P.J.A. Kenis, Effect of cations on the electrochemical conversion of CO_2 to CO, J Electrochem. Soc. 160 (2013) F69–F74.
[23] D.T. Whipple, E.C. Finke, P.J.A. Kenis, Microfluidic reactor for the electrochemical reduction of carbon dioxide: the effect of pH, Electrochem. Solid State Lett. 13 (2010) B109–B111.
[24] J. Resasco, Y. Lum, E. Clark, J.Z. Zeledon, A.T. Bell, Effects of anion identity and concentration on electrochemical reduction of CO2, Chemelectrochem 5 (2018) 1064–1072.
[25] H.R.M. Jhong, C.E. Tornow, C. Kim, S. Verma, J.L. Oberst, P.S. Anderson, A.A. Gewirth, T. Fujigaya, N. Nakashima, P.J.A. Kenis, Gold nanoparticles on polymer-wrapped carbon nanotubes: an efficient and selective catalyst for the electroreduction of CO_2, ChemPhysChem 18 (2017) 3274–3279.
[26] A. Schizodimou, G. Kyriacou, Acceleration of the reduction of carbon dioxide in the presence of multivalent cations, Electrochim. Acta 78 (2012) 171–176.
[27] G. Hussain, L. Pérez-Martínez, J.B. Le, M. Papasizza, G. Cabello, J. Cheng, A. Cuesta, How cations determine the interfacial potential profile: relevance for the CO_2 reduction reaction, Electrochim. Acta 327 (2019) 135055.
[28] M.M. Waegele, C.M. Gunathunge, J. Li, X. Li, How cations affect the electric double layer and the rates and selectivity of electrocatalytic processes, J. Chem. Phys. 151 (2019) 160902.
[29] https://www.southernionics.com/pdf/pb/PB184_Aluminum_Chloride_Solution_Technical_Grade_A.pdf (Accessed: 15 April 2021).
[30] https://www.engineeringtoolbox.com/density-aqueous-solution-inorganic-chlorides-salt-concentration-d_1955.html (Accessed: 15 April 2021).
[31] H.R.M. Jhong, F.R. Brushett, P.J.A. Kenis, The effects of catalyst layer deposition methodology on electrode performance, Adv. Energy Mater. 3 (2013) 589–599.
[32] M.S. Naughton, A.A. Moradia, P.J.A. Kenis, Quantitative analysis of single-electrode plots to understand *in-situ* behavior of individual electrodes, J. Electrochem. Soc. 159 (2012) B761–B769.
[33] A. Sacco, Electrochemical impedance spectroscopy as a tool to investigate the electroreduction of carbon dioxide: a short review, J. CO2 Utilization 27 (2018) 22–31.
[34] F. Bienen, D. Kopljar, A. Löwe, S. Geiger, N. Wagner, E. Klemm, K.A. Friedrich, Revealing mechanistic processes in gas-diffusion electrodes during CO_2 re-

duction via impedance spectroscopy, ACS Sustain. Chem. Eng. 8 (2020) 13759–13768.
[35] F. Bienen, D. Kopljar, S. Geiger, N. Wagner, K.A. Friedrich, Investigation of CO_2 electrolysis on tin foil by electrochemical impedance spectroscopy, ACS Sustain. Chem. Eng. 8 (2020) 5192–5199.
[36] M. Dunwell, W. Luc, Y. Yan, F. Jiao, B. Xu, Understanding surface-mediated electrochemical reactions: CO_2 reduction and beyond, ACS Catal. 8 (2018) 8121–8129.
[37] J. Gu, C.S. Hsu, L. Bai, H.M. Chen, X. Hu, Atomically dispersed Fe^{3+} sites catalyze efficient CO_2 electroreduction to CO, Science 364 (2019) 1091.
[38] A. Jain, S.P. Ong, G. Hautier, W. Chen, W.D. Richards, S. Dacek, S. Cholia, D. Gunter, D. Skinner, G. Ceder, K.A. Persson, Commentary: the materials project: a materials genome approach to accelerating materials innovation, APL Mater. 1 (2013) 011002.
[39] K.A. Persson, B. Waldwick, P. Lazic, G. Ceder, Prediction of solid-aqueous equilibria: scheme to combine first-principles calculations of solids with experimental aqueous states, Phys. Rev. B 85 (2012) 235438.
[40] A.K. Singh, L. Zhou, A. Shinde, S.K. Suram, J.H. Montoya, D. Winston, J.M. Gregoire, K.A. Persson, Electrochemical stability of metastable materials, Chem. Mater. 29 (2017) 10159–10167.
[41] Z. Wu, Y. Shen, Y. Dong, J. Jiang, Study on the morphology of α-Al2O3 precursor prepared by precipitation method, J. Alloys Compd. 467 (1–2) (2009) 600–604 https://www.sciencedirect.com/science/article/pii/S0925838808000091.
[42] C.A. Handwerker, P.A. Morris, R.L. Coble, Effects of chemical inhomogeneities on grain growth and microstructure in Al_2O_3, J. Am. Ceram. Soc. 72 (1989) 130–136.
[43] K. Cui, L. Liu, F. Ma, M. Jing, Z. Li, Y. Tong, M. Sun, S. Li, J. Zhang, Y. Zhang, Enhancement of thermal conductivity of $Ba(OH)_2$ $8H_2O$ phase change material by graphene nanoplatelets, Mater. Res. Express 5 (2018) 065522.
[44] L. Hoseini, B.A. Gh, Effect of the amount of BaO catalyst on the selective acetylation of benzyl alcohols and doxycycline degradation, Chem. Afr. 2 (2019) 377–382.
[45] K.M. Saoud, I. Ibala, D.E. Ladki, S. Saeed, O. Ezzeldeen, Microwave assisted preparation of calcium hydroxide and barium hydroxide nanoparticles and their application for conservation of cultural heritage, in: Proceedings of the Euro Mediterranean Conference, 2014.
[46] Z. Mirghiasi, F. Bakhtiara, E. Darezereshki, E. Esmaeilzadeh, Preparation and characterization of CaO nanoparticles from $Ca(OH)_2$ by direct thermal decomposition method, J. Ind. Eng. Chem. 20 (2014) 113–117.
[47] M.A.O. Mydin, Preliminary studies on the development of lime-based mortar with added egg white, Int. J. Technol. 5 (2017) 800–810.
[48] J.J. Kaczur, H. Yang, Z. Liu, S.D. Sajjad, R.I. Masel, Carbon dioxide and water electrolysis using new alkaline stable anion membranes„ Front. Chem. 6 (2018) 263 https://www.frontiersin.org/articles/10.3389/fchem.2018.00263/full.
[49] R.B. Kutz, Q. Chen, H. Yang, S.D. Sajjad, Z. Liu, I.R. Masel, Sustainion imidazolium-functionalized polymers for carbon dioxide electrolysis, Energy Technol. 5 (2017) 929–936.
[50] S. Banerjee, Z.Q. Zhang, A.S. Hall, V.S. Thoi, Surfactant perturbation of cation interactions at the electrode–electrolyte interface in carbon dioxide reduction, ACS Catal. 10 (2020) 9907–9914.
[51] Z.Q. Zhang, S. Banerjee, V.S. Thoi, A. Shoji Hall, Reorganization of interfacial water by an amphiphilic cationic surfactant promotes CO_2 reduction, J. Phys. Chem. Lett. 11 (2020) 5457–5463.
[52] E.R. Cofell, U.O. Nwabara, S.S. Bhargava, D.E. Henckel, P.J.A. Kenis, Investigation of electrolyte-dependent carbonate formation on gas diffusion electrodes for CO_2 electrolysis, ACS Appl. Mater. Interfaces 13 (2021) 15132–15142.
[53] S. Ringe, C.G. Morales-Guio, L.D. Chen, M. Fields, T.F. Jaramillo, C. Hahn, K. Chan, Double layer charging driven carbon dioxide adsorption limits the rate of electrochemical carbon dioxide reduction on Gold, Nat. Commun. 11 (2020) 33.
[54] X. Chen, M.S.G. Ahlquist, Deconstructing the enhancing effect on CO_2 activation in the electric double layer with EVB dynamic reaction modeling, J. Phys. Chem. C 124 (2020) 22479–22487.
[55] D. Bohra, J.H. Chaudhry, T. Burdyny, E.A. Pidko, W.A. Smith, Modeling the electrical double layer to understand the reaction environment in a CO_2 electrocatalytic system, Energy Environ. Sci. 12 (2019) 3380–3389.
[56] J.A. Banda-Alemán, G. Orozco, E. Bustos, S. Sepúlveda, J. Manríquez, Double-layer effect on the kinetics of CO_2 electroreduction at cathodes bearing Ag, Cu, and Ag/Cu nano-arrays electrodeposited by potentiostatic double-pulse, J. CO2 Utilization 27 (2018) 459–471.
[57] S. Wallentine, S. Bandaranayake, S. Biswas, L.R. Baker, Direct Observation of carbon dioxide electroreduction on gold: site blocking by the stern layer controls CO_2 adsorption kinetics, J. Phys. Chem. Lett. 11 (2020) 8307–8313.
[58] Y. Zhang, J. Tang, Z. Ni, Y. Zhao, F. Jia, Q. Luo, L. Mao, Z. Zhu, F. Wang, Real-time characterization of the fine structure and dynamics of an electrical double layer at electrode–electrolyte interfaces, J. Phys. Chem. Lett. 12 (2021) 5279–5285.